Applied Geochemistry 97 (2018) 247–255

Contents lists available at ScienceDirect

Applied Geochemistry

journal homepage: www.elsevier.com/locate/apgeochem

Geochemical and mineralogical characterization of the arsenic-, iron-, and sulfur-rich mining waste dumps near Kaňk, Czech Republic

Helena Jelenová[a], Juraj Majzlan[b], Felix Y. Amoako[b], Petr Drahota[a,*]

[a] Institute of Geochemistry, Mineralogy and Mineral Resources, Faculty of Science, Charles University, Albertov 6, 128 43, Prague 2, Czech Republic
[b] Institute of Geosciences, Friedrich-Schiller University, Burgweg 11, D-07749, Jena, Germany

ARTICLE INFO

Editorial handling by Prof. M. Kersten

Keywords:
Medieval mining waste
Arsenic
Bukovskýite
As-HFO
Mobility

ABSTRACT

The role of secondary minerals in controlling the migration of arsenic and selected metals (Cu, Pb, Zn) has been investigated in voluminous mining waste dumps at Kaňk (northern part of the Kutná Hora ore district, Czech Republic). These wastes initially contained a large amount of Fe sulfides and arsenopyrite and have been exposed to atmosphere for approximately 500 years. The long-term weathering under acidic conditions caused dissolution of almost all sulfides and significant alteration of primary silicate minerals, producing deeply weathered As-, Fe-, and S-rich waste material (As: 13 g kg^{-1}; Fe: 74 g kg^{-1}; S: 44 g kg^{-1}) with large proportion of clayey matrix filling the space between rock fragments. Detailed mineralogical investigation (powder X-ray diffraction, electron microprobe, Raman spectroscopy) and sequential extraction revealed that arsenic in these wastes is principally stored in reactive but not highly soluble minerals such as poorly-crystalline Fe (oxyhydr) oxides, bukovskýite, and X-ray amorphous hydrated ferric arsenate (HFA). Lesser fraction of As is contained in schwertmannite and less reactive scorodite, jarosite, and well-crystalline Fe (oxyhydr)oxides (especially goethite). Fe (oxyhydr)oxides also appear to be the main reservoirs of Cu and Zn; Pb is principally stored in jarosite. Acidic pore waters (pH ≈ 2.8) collected after rainfall events contain much Al (113 mg L^{-1}), As (2.5 mg L^{-1}), Ca (500 mg L^{-1}), Cu (24 mg L^{-1}), Fe (58 mg L^{-1}), Si (44 mg L^{-1}), SO_4^{2-} (2170 mg L^{-1}) and Zn (16 mg L^{-1}). Geochemical modeling revealed that most of these elements (Al, Ca, Cu, SO_4^{2-}, Zn) are controlled by ephemeral Al-Ca-Cu-Zn sulfates (e.g. gypsum, aluminite), which form at the surface of the waste dumps as a result of evaporation of pore solutions during dry seasons. Despite the fact that bukovskýite and other interesting Fe(III) (sulfo)arsenate minerals store a major part of As in the mining wastes, geochemical modeling supported the notion that mobility of As and Fe is controlled by the unspectacular poorly-crystalline As-bearing Fe (oxyhydr) oxides. The data show that the Fe(III) (oxyhydr)oxides, (sulfo)arsenates and hydroxysulfates in the 500-year-old mining waste dump retain arsenic efficiently but not completely. Monitoring wells installed at the site before our research recorded up to 1440 mg L^{-1} As in shallow groundwater. They argue, however, that this aquifer is disconnected from the larger groundwater bodies at the site and hence does not represent arsenic accumulation of environmental concern.

1. Introduction

Abandoned mine wastes contain high sulfide concentrations and are among the most serious sources of environmental pollution. Pore waters in mine effluents from sulfide-rich waste are generally characterized by low pH values and high concentrations of various metals and metalloids (Blowes et al., 2013; Jambor, 2003). The weathering of wastes with high contents of pyrite (FeS_2) or pyrrhotite ($Fe_{1-x}S$) and simultaneously copious arsenopyrite (FeAsS) may develop acidic weathering solutions which attain great concentration of Fe and As, and above all, enormous concentrations of SO_4^{2-} (Casiot et al., 2003; Gieré et al., 2003; Nordstrom et al., 2000; Williams, 2001). Characteristic compounds of the secondary As mineral assemblage formed from these aqueous solutions include Fe(III) (oxyhydr)oxides, (hydroxy)sulfates, and (sulfo)arsenates or (sulfo)arsenites (Drahota and Filippi, 2009; Majzlan et al., 2014). The formation or dissolution of these mineral phases may be enhanced by the metabolic activity of bacteria. Field evidence and laboratory studies conducted in the Carnoulès acid mine drainage system suggest that As(III)- and As(V)-bearing minerals phases form *via* distinct mechanisms: oxidation of Fe(II) without As(III) oxidation, for example, by the *Acidithiobacillus ferrooxidans* leads to the formation of tooeleite ($Fe_6(AsO_3)_4SO_4(OH)_4{\cdot}H_2O$) (Duquesne et al.,

* Corresponding author.
E-mail addresses: petr.drahota@natur.cuni.cz, drahota@natur.cuni.cz (P. Drahota).

https://doi.org/10.1016/j.apgeochem.2018.08.029
Received 19 July 2018; Received in revised form 27 August 2018; Accepted 30 August 2018
Available online 01 September 2018

2003; Egal et al., 2006), while oxidation of both Fe(II) and As(III), for example by *Thiomonas* sp. leads to the formation of As(V)-Fe(III) hydroxysulfates (Morin et al., 2003). Understanding the biogeochemical processes which control the precipitation and dissolution of secondary As minerals in abandoned mine wastes is crucial for formulation of models that predict the environmental impact of these sites. Moreover, a better knowledge of these mechanisms will allow remediation of these sites and/or reduction of the extent of future pollution.

Gold and silver mining conducted during the Middle Ages throughout Europe has left an environmental legacy of waste dumps containing high levels of As. At Kaňk (Kutná Hora ore district, Czech Republic), nearly 5 million metric tons of silver and copper ores were processed between 14th and 17th century and resulting waste was deposited at the sites of mining (Malec and Pauliš, 1997). This material contained large amount of sulfides dominated by arsenopyrite, pyrite, pyrrhotite, and sphalerite (ZnS). Sulfides have succumbed to oxidation since they were dumped under surface conditions. Such processes generated acidic solutions rich in As, Fe, and S and formed a unique paragenesis of secondary As phases including abundant amorphous hydrated ferric arsenate (HFA), scorodite ($FeAsO_4{\cdot}2H_2O$), and bukovskýite ($Fe_2(AsO_4)(SO_4)(OH){\cdot}9H_2O$), minor kaňkite ($FeAsO_4{\cdot}3.5H_2O$), and rare zýkaite ($Fe_4(AsO_4)_3(SO_4)(OH){\cdot}15H_2O$) and parascorodite ($FeAsO_4{\cdot}2H_2O$) (Čech et al., 1976, 1978; Novák et al., 1967; Ondruš et al., 1999).

The deposition and long-term weathering of sulfide-rich waste at Kaňk provides a unique field-scale laboratory for examination of the behavior and potential mechanism(s) of release of arsenic into pore waters in the late paragenetic stage of mining waste development, after consumption of most of the primary sulfides. In this study, approximately 500-years old mining waste from three profiles and pore waters were examined to determine (1) vertical variations in the mineralogy of the arsenic (and other potentially toxic elements) carriers by powder X-ray diffraction, electron microprobe, and Raman spectroscopy, (2) solubility-controlling phases that command the sequestration and release of these elements, by sequential extraction and pore-water chemistry, and (3) long-term behavior of metals and metalloids, relevant to the long-term fate of more recent, modern mining waste in the future. These data were used to elucidate major modes of As bonding in the solid phase, and to explain the As solid-water partitioning under strongly acidic to neutral conditions in the mining waste dump at Kaňk.

2. Study site

The hydrothermal Ag-Pb-Zn-Cu ore deposits at Kaňk are located in the northern periphery of Kutná Hora ore district, one of the best known European mining centers of the Middle Ages. The Kutná Hora ore district comprises a system of subparallel ore veins and ore zones associated with faults in regionally metamorphosed rocks of the Kutná Hora complex (Holub et al., 1982) built by biotite-muscovite gneisses and migmatites intercalated with amphibolites, eclogites, and serpentinites. The Staročeské ore zone in the northern part of the district was one of the main vein zones in this district. The intensive mining and processing activities in this zone in the first half of 16th century left a legacy of large waste dumps (average area of 3000 m^2, with thickness up to 20 m, individually; totaling a few hundred thousand tons), which are concentrated in an area of ~1500 × 200 m, elongated along the N-S direction (from the northern to the southern border of the village of Kaňk) (Fig. 1).

The waste dump materials in the Staročeské ore zone are heterogeneous, with particles ranging from very fine (clay) to coarse (tens of cm), including barren gneiss host rock and hydrothermally altered and mineralized rocks. The waste dumps are characterized by high to extreme levels of As (up to 2.68 wt.%) while the contents of Cu (up to 0.1 wt.%), Pb (up to 0.03 wt.%), and Zn (up to 0.1 wt.%) are typically one to two orders of magnitude lower (Kocourková-Víšková et al., 2015). More recent mineralogical studies (Drahota et al., 2018; Kocourková-Víšková et al., 2015; Majzlan et al., 2012b) showed that As in the mining waste precipitates as (sulfo)arsenate minerals but also found that large fraction of As is adsorbed and/or coprecipitated with minerals of jarosite subgroup ($\sim A Fe_3(SO_4)_2(OH)_6$, where A: Na^+, K^+, H_3O^+, $0.5\,Pb^{2+}$), schwertmannite ($\sim Fe_8O_8(OH)_6SO_4$) and Fe(III) (oxyhydr)oxides. Rainwater percolating through the mining wastes leaches pollutants from these secondary phases and probably seeps into and contaminates shallow groundwater. Chemical composition of the groundwater contained in the shallow aquifers is highly variable, but can be locally very acidic (pH 1.39) and attaining up to 1440 mg L^{-1} As, 10 g L^{-1} Fe, and 28.6 g L^{-1} SO_4^{2-} (Čížek et al., 2012; Havlíček and Pácal, 1962; Raus et al., 2011).

The Kutná Hora ore district is located in an undulating landscape (an altitude of 260 m above sea level). The average annual temperature is 8.5 °C, and the total precipitation averages 580 mm.

3. Materials and methods

3.1. Materials

The waste material from the historical mining waste dumps were sampled in two excavation pits A (49°58′34.267″N, 15°16′8.164″E) and B (49°58′49.830″N, 15°16′9.851″E) and in an outcrop in a steep side slope (C) (49°58′44.664″N, 15°16′4.791″E) of the waste piles (Fig. 1). The waste samples (n = 19) were collected and composited along each profile in discrete depth intervals (30–80 cm) distinguished visually (color, consistency) from other parts of the profiles. The solids were collected using a stainless steel hand trowel, sealed in plastic bags and transported to the laboratory. In the laboratory, the samples were air dried, homogenized, and sieved. The fraction < 2 mm was used for chemical and mineralogical analyses. Mineralogical investigation, principally an electron microprobe study, also involved larger fragments of waste rock as well as nodules of bukovskýite, which commonly achieve cm-scale dimensions (Majzlan et al., 2012b).

Pore waters (n = 23) were sampled with Rhizon tension lysimeters (100-mm long porous nylon polymer membrane with a mean pore size 0.1 μm) that were installed in the outcrop intervals previously used for collection of the solid samples (C profile). The pore-water samples were collected after rainy days in October 2014 and April 2015. Completely wet mining waste material in the outcrop enabled collection of the pore water samples (~15 mL) within 2–5 h.

3.2. Characterization

The physically bound water content of each solid sample was determined as weight loss after keeping the sample for 24 h at 105 °C. Combination of sieving and hydrometer method was used for an estimation of particle size distribution. The pH was measured in a 1:2.5 (w/v) solid-deionized water suspension after 1 h of agitation, using a combined pH electrode and WTW multimeter.

For bulk chemical and phase analyses, an aliquot of each sample was ground to analytical fineness in an agate planetary ball mill. Homogenized waste samples were analyzed for total element concentrations by energy-dispersive X-ray fluorescence (XRF) spectrometry (ARL 9400 XP^+, Thermo ARL). The accuracy for major and trace elements was within 2% and 5%, respectively, based on the analyses of a standard reference material (NIST 2710a). The content of total organic carbon (TOC) and total inorganic carbon (TIC) was determined using a combination of ELTRA CS 530 and ELTRA CS 500 TIC analyzers.

The heavy fractions of selected samples (n = 6; two samples from each mining waste profile) were concentrated in 1,1,2,2-tetrabromoethane (specific gravity of 2.93 g cm^{-3}). Heavy-grain concentrates, bulk samples as well as selected waste rock fragments and bukovskýite nodules were prepared for the electron microprobe analyses and Raman microspectrometry in the form of polished sections. Mineralogy of all samples was investigated by powder X-ray diffraction

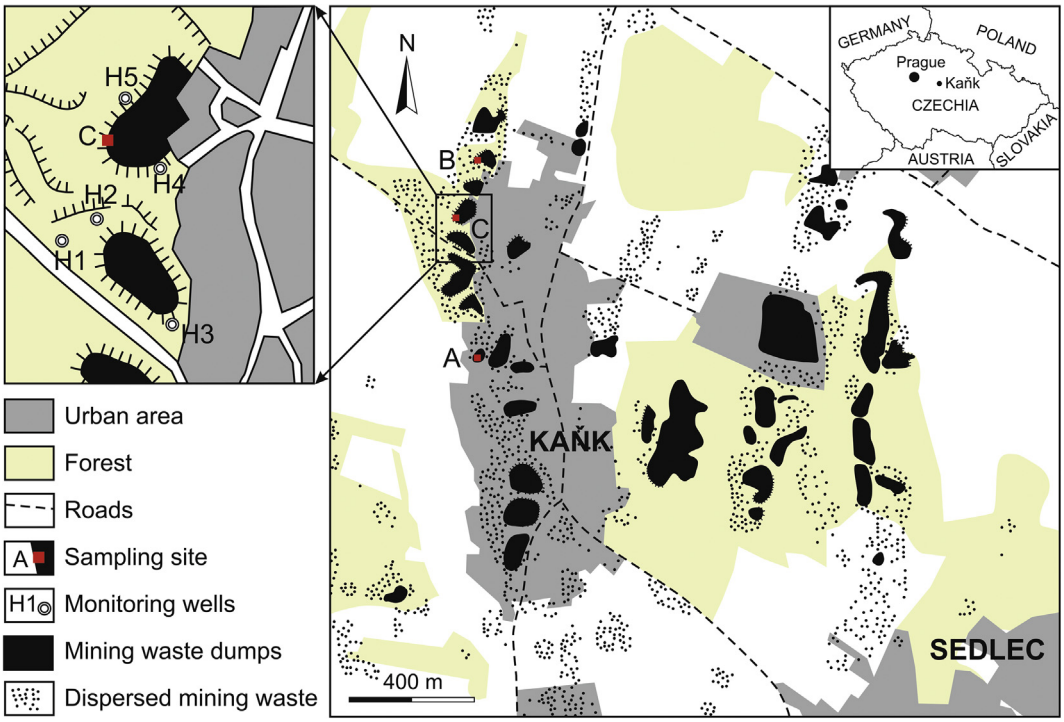

Fig. 1. Schematic map of the historical mining site of Kaňk showing a) the location of sampling sites (shown as red squares), b) wells previously used for monitoring groundwater chemistry (Čížek et al., 2012; Raus et al., 2011), and c) inset location of the mining site in central Europe. Modified after Malec and Pauliš (1997). (For interpretation of the references to color in this figure legend, the reader is referred to the Web version of this article.)

(XRD) analysis. XRD patterns were collected with a PANalytical X'Pert Pro diffractometer, in Bragg-Brentano geometry, using Cu Kα radiation (40 kV and 30 mA), a diffracted-beam monochromator, and an X'Celerator multichannel detector. The diffraction data were analyzed using PANalytical X'Pert HighScore software, version 3.0e.

Chemical compositions of the individual grains were determined with a Cameca SX100 electron microprobe (EMP) (Prague) under the operating condition of 15 kV, 10 nA, and a beam diameter of 2 μm or with JEOL JXA-8230 electron microprobe (Jena) with an accelerating voltage 15 kV, sample current of 15 nA, 30 s on each peak and 30 s on the background, and beam diameter of 5 μm. Details of the analytical conditions (X-ray lines and standards) are listed in Table S1.

Raman microspectrometric (RMS) analyses were performed on selected grains and their spots previously explored by EMP (locations of RMS spot analyses in the grains were almost identical to EMP spots) using a Renishaw InVia Reflex Raman spectrometer (Renishaw plc, UK) coupled with a Leica microscope (Leica Microsystems, Germany) using a 50× objective. Excitation was provided by the 514.5 nm line of a diode laser. Spectrum of each mineral was recorded at 5% laser power, ~5 mW, to avoid thermal degradation, over the spectral range of 100–1200 cm^{-1}. Scanning parameters were as follows: 20 s accumulation time and 3–20 scans were taken to improve the signal-to-noise ratio.

A five step sequential extraction procedure (SEP) of Drahota et al. (2014) was employed to determine the partitioning of arsenic in the mining waste samples, targeting (F1) water-soluble As, (F2) specifically sorbed As fraction, As associated with (F3) poorly-crystalline as well as (F4) crystalline Fe(III) (hydr)oxides, hydroxysulfates and (sulfo)arsenates, and (F5) As associated with sulfides and (sulf)arsenides. The samples were centrifuged after each extraction step, filtered using a nylon 0.2 μm membrane filter, and acidified by adding 1 M HNO_3 before As and Fe analysis. Every fifth extraction was performed in duplicate, showing a standard deviation of < 5% for As and Fe except for two analyses in the last SEP step which showed 11% and 14%; a procedural blank was run during the extraction procedures. The accuracy of the SEP was tested by comparing the pooled amount of As recovered from all of the fractions (F1-F5) against the total As concentrations obtained by XRF. The correlation between both values is highly significant (R^2 = 0.98; p < 0.0001); the recoveries were acceptable (90–110%).

Pore-water samples were analyzed not later than 4 h after the collection in the field. The variable determined were pH (by combined microelectrode, calibrated by pH 1.679, 4.006, and 6.865 buffer solutions), Eh (by Pt microelectrode, following the procedure outlined in Nordstrom and Wilde, 2005), Fe(II) and total Fe using portable DR3900 spectrophotometer (HachLange). Fe(II) concentrations were determined using the Hach 1,10-phenanthroline method. The concentration of total pore water Fe was also determined using this method, following pre-reduction of Fe(III) by ascorbic acid. The major cations and trace elements were determined using inductively-coupled plasma optical emission spectrometry (ICP-OES; Agilent 5100), and inductively-coupled plasma mass spectrometry (ICP-MS; Thermo Scientific Xseries^{II}), respectively. The major anions were determined using a Dionex ICS-2000 ion chromatography system. The measured concentrations of elements in the certified standards (CertiPUR®) were generally within ± 2% of their certified values.

3.3. Geochemical modeling

The PHREEQC-2 geochemical speciation-solubility code, version 2.13.2 for Windows (Parkhurst and Appelo, 1999) was used to determine the degree of saturation of waste pore water with respect to the Fe (oxyhydr)oxides, (hydroxy)sulfates, and (sulfo)arsenates. The Wateq4f thermodynamic database was supplemented by the solubility products of amorphous ferric arsenate (Langmuir et al., 2006), bukovskýite (Majzlan et al., 2012b), kaňkite and scorodite (Majzlan et al., 2012a), lepidocrocite (taken from Minteq. v4 thermodynamic database), schwertmannite (Yu et al., 1999), and zýkaite (Majzlan et al., 2015).

4. Results

4.1. Physical and chemical characteristics

The mining waste profiles A, B, and C are located in the dumps of historical mines of Rabštejn, Trmandl (exploitation ceased in 1550), and Šafary (exploitation flourished until the end of the 16th century), respectively (Kořan, 1950), all belonging to the Staročeské ore zone. The mining wastes consist of highly heterogeneous material with large fragments of heavily weathered rocks (up to 20 cm) in a fine-grained matrix (clay and silt: 10–34%), often cemented together by secondary matter. Pieces of anthropogenic material such as charcoal and burnt clay, which are all related to medieval mining technologies, are relatively common.

The deepest samples of each profile were similar to the oxidized surface samples. They exhibited no visual evidence of reductive conditions as well as moistening. Most mining waste samples had brownish yellow color and strongly acidic pH (2.7–3.1); the situation was different in profile B, where the pH ranged from acidic to neutral (4.4–7.1). The acidity generated by the decomposing sulfides in this profile has been probably neutralized by Cretaceous marine carbonates that are occasionally present in the waste material of the dumps (Drahota et al., 2018). However, very low contents of TIC (always below 0.1 wt.%) suggest that carbonates have been completely consumed in all studied samples.

A detailed description and properties of the studied mining wastes are reported in Table S2. Chemical composition of the mining wastes reflects the compositions of ores mined. The waste samples are very rich in Fe (49.3–92.9 g kg^{-1}, $\bar{x}$: 74.2 g kg^{-1}) and S (8.3–55.7 g kg^{-1}, $\bar{x}$: 43.9 g kg^{-1}). Arsenic is by far the most significant trace metal(loid) in all samples studied (5.6–22.0 g kg^{-1}, $\bar{x}$: 13.2 g kg^{-1}), while other potential trace metals such as Cu ($\leq$0.47 g kg^{-1}, $\bar{x}$: 0.28 g kg^{-1}), Pb ($\leq$0.51 g kg^{-1}, $\bar{x}$: 0.20 g kg^{-1}), Sn ($\leq$2.00 g kg^{-1}, $\bar{x}$: 0.83 g kg^{-1}), and Zn ($\leq$2.54 g kg^{-1}, $\bar{x}$: 0.54 g kg^{-1}) have much lower concentrations, implying lower proportion of their sulfides relative to Fe sulfides and arsenopyrite in the parental waste material. Although Fe-bearing sulfides (pyrite, pyrrhotite, and arsenopyrite) obviously dominated in the parental waste material, bulk concentrations of S in the waste samples do not correlate with Fe. Sulfur significantly correlates with Ca (R^2 = 0.73, p < 0.001), Fe accompanies As (R^2 = 0.55, p < 0.001). Variations in the chemical concentration of Fe, S, and trace metal(loid)s between and along the profiles (Table S2) suggest that the proportion of sulfides in the parental waste material differed both spatially and in time of deposition. Lower Fe ($\bar{x}$: 62.2 g kg^{-1}), S ($\bar{x}$: 28.2 g kg^{-1}) and higher Zn ($\bar{x}$: 1.74 g kg^{-1}) concentrations in the profile B in comparison to profiles A and C indicate lower proportion of Fe sulfides as well as higher proportion of sphalerite in the ore of the Trmandl mine. Variability of As, Cu, Pb, Sn, and Zn along the profiles corresponds likely to variations in the primary minerals of these metal(loid)s in the deposited waste.

4.2. Mineralogy

The secondary arsenical phases occur as discrete particles sometimes displaying zoning and banding or as complex intergrowths (Fig. 2). The intimate association of Fe (oxyhydr)oxides, hydroxysulfates, and (sulfo)arsenates in successive bands and zones (Fig. 2) is suggestive of precipitation and co-precipitation over small distances.

Bulk powder XRD patterns showed that the major minerals in the < 2 mm fraction of all mining waste samples are muscovite/illite and quartz and the minor minerals are gypsum, jarosite, K-feldspar and plagioclase. Field observation revealed that upper parts of the profiles (A: depth of 40–120 cm; C: depth of 60–180 cm) are also rich in bukovskýite, forming usually cm-sized nodules in the fine-grained, silicate-dominated matrix. Bukovskýite is commonly accompanied by X-ray amorphous substance with very variable composition whose major elements may include Fe, As, S, Si, or Al. These 'gels' (cf. Majzlan et al., 2012b) are not voluminous but probably have elevated solubility of arsenic and other elements. The powder XRD investigation of the heavy mineral fractions (> 2.93 g cm^{-3}), which were separated from two most contrasting samples (with respect to depth, pH, and As concentration) of each profile, indicated presence of Fe(III) oxides (goethite, hematite and lepidocrocite) and also identified scorodite in the mining waste profile B (Fig. S1).

The primary rock-forming silicates and gypsum contain no arsenic. Gypsum conforms essentially to its nominal stoichiometry. The only metal other than Ca that occasionally exceeds the detection limit of the analyses is Cu (up to 0.12 wt.% CuO).

A detailed electron microprobe study of the secondary As-bearing phases indicated that the principal arsenic carriers are Fe(III) (oxyhydr) oxides, Fe(III) hydroxysulfates, and Fe(III) (sulfo)arsenates, accounting for ≈95% of the As-bearing mineral grains examined ($n \approx 1700$, Fig. 3a). Because of the inability of the electron microprobe to analyze water content, variable stoichiometry of some of the phases and polymorphism, the final identification of the abundant arsenic carriers was done in combination with Raman spectroscopy (Fig. 3b). The minor to trace As-bearing phases include primary arsenopyrite, a secondary As_4S_4 phase, As oxide, Pb-As oxide, and an unknown secondary Fe-As-Sn oxide (Fig. S2). They occur in trace amounts and thus are not considered to have a notable environmental significance at the studied site. The scarcity of primary sulfides in the profiles as well as polished sections indicates that secondary phases are product of a complete replacement of the ores.

Most of the Fe arsenates are characterized by sharp, well-resolved, intense Raman bands (spectrum R1; Fig. S3), at positions corresponding well to the references values of scorodite (Culka et al., 2016; Filippi et al., 2009). EMP spots confirmed by Raman spectroscopy as scorodite (n = 7) show nearly equal molar contents of Fe and As (Fe/As ~ 1.09) and low concentrations of S (0.2–2.7 wt.% of SO_3). Among the other analyses assumed to represent scorodite, sulfur was detected in the same concentration (mostly between 0.8 and 2.4 wt.% SO_3, n = 349). Most of the analyzed spots show P_2O_5 of 0.0–1.0 wt.%, with only a few analyses deviating up to 4.7 wt.% P_2O_5. PbO content is usually near or below detection limit, with only a few data points with up 0.7 wt.% PbO. Analyses with elevated PbO show essentially no P_2O_5 and vice versa.

Sulfur-rich Fe arsenates (7.7–8.1 wt.% SO_3; n = 3) displayed two broad Raman bands similar to those reported for amorphous HFA (Culka et al., 2016; Drahota et al., 2016; Filippi et al., 2009). EMP analyses of grains identified by RMS as HFA show prevalence of Fe over As (average molar ratio Fe/As of 1.99). The lack of As is slightly compensated by substitution of S and P (average 8.0 wt.% SO_3 and 1.5 wt.% P_2O_5); however, average molar Fe/(As, S, P) ratio in HFA of 1.4 still displays nonstoichiometric composition of the major elements just as in other studies (Drahota et al., 2016; Dunn, 1982; Filippi et al., 2015; Gieré et al., 2003).

All Fe sulfoarsenates were identified by Raman spectroscopy (spectrum R1; Fig. S3) as bukovskýite (Culka et al., 2016; Loun et al., 2011). The chemical composition of this mineral corresponds to almost pure and stoichiometric bukovskýite (cf. Majzlan et al., 2012b), with low P concentrations (up to 2.8 wt.% P_2O_5, n = 5, spots confirmed by RMS). Other analyses assumed to represent bukovskýite show similar P concentrations, with a few outliers with up to 6.0 wt.% P_2O_5.

Fe(III) hydroxysulfates are another dominant group of As-bearing secondary phases in the mining waste at Kaňk. Two groups of phases were distinguished with Raman spectroscopy: jarosite subgroup minerals (Raman spectrum R4; Fig. S3) and schwertmannite (Raman spectrum R5; Fig. S3). Chemical compositions of jarosite subgroup minerals correspond to jarosite or natrojarosite, with a minor amount of the hydroniumjarosite and plumbojarosite components. Content of As in these minerals is always below 3.8 wt.% As_2O_5, with an average of 1.1 wt.% (n = 3 confirmed by RMS or n = 212 for all analyses). Higher

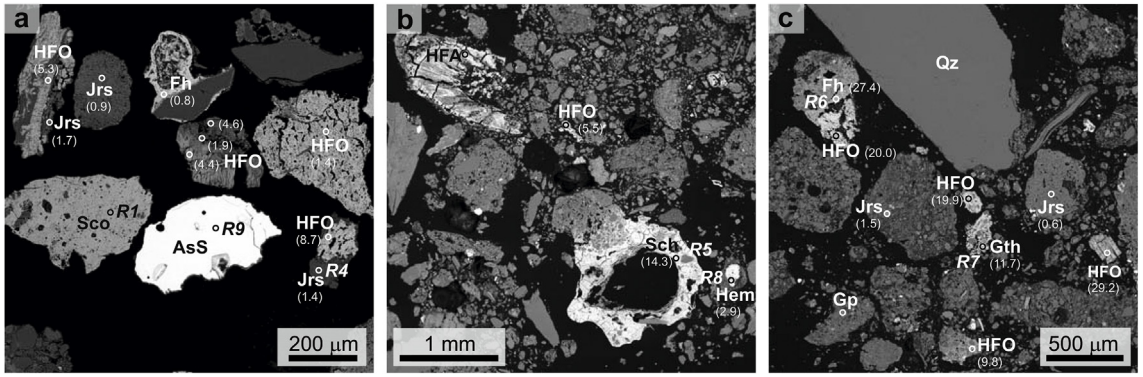

Fig. 2. Back-scattered electron (BSE) images of secondary arsenic minerals from Kaňk showing a) discrete particles of As minerals in the heavy mineral fraction as well as (b, c) complex aggregates of aluminosilicates and As minerals in the bulk samples. Arsenic concentrations in parentheses are expressed in wt.% As_2O_5. Raman spectra obtained from locations *R1* and *R4-R9* are given in (Fig. S3). Fh - ferrihydrite; Gp - gypsum; Gth - goethite; Hem - hematite; HFA – amorphous hydrated ferric arsenate; HFO – unidentified Fe (oxyhydr)oxide; Jrs - jarosite; Qz - quartz; Sch - schwertmannite; Sco - scorodite.

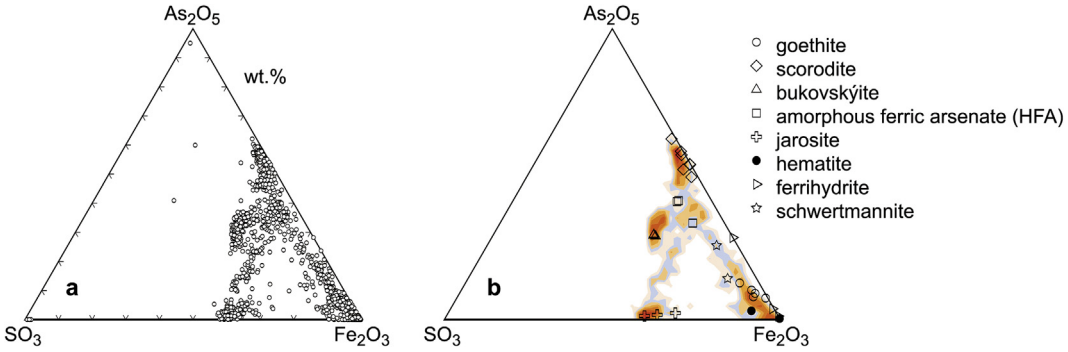

Fig. 3. a) Chemical composition of the secondary minerals from Kaňk (all data from spot analyses from the electron microprobe, $n \approx 1700$); b) density of the spot analyses from a) shown by a contour plot and overlain by symbols for the spots where the minerals were identified by Raman spectroscopy.

concentrations of As were detected in less abundant schwertmannite (up to 23.0 wt.% As_2O_5; $n = 2$). As a result of the appreciable As content, RMS of schwertmannite exhibit distinct As(V)–O stretching band at about 850 cm^{-1} (Fig. S3; cf. Burton et al., 2009).

Fe(III) (oxyhydr)oxides were identified by Raman spectroscopy as ferrihydrite, goethite, and hematite (Raman spectra R6, R7, and R8, respectively; Fig. S3); lepidocrocite, identified in minor amount in heavy mineral fractions by powder XRD, was not detected by Raman spectroscopy. EMP analyses of grains identified by RMS as ferrihydrite ($n = 4$) displayed highly variable content of As (0.1–27.4 wt.% of As_2O_5) as well as trace metals (≤10.4 wt.% of CuO, ≤24.0 wt.% of ZnO). Goethite contains also much As (6.6–11.7 wt.% As_2O_5; $n = 5$) and slightly increased content of Zn ($\bar{x}$: 0.5 wt.% ZnO; $n = 5$). Very high As contents in ferrihydrite as well as goethite are consistent with the spectral feature at ~850 cm^{-1} (Raman spectra R6 and R7; Fig. S3) that is assigned to the As-O stretching vibration of the bidentate-complexed arsenate (Jia et al., 2006). In contrast, As(V)-O stretching band at 826 cm^{-1} (Das et al., 2014) or 866 cm^{-1} (Müller et al., 2010), previously documented in As-loaded hematite, is not noticeable in our spectra of hematite (Raman spectra R8; Fig. S3). This is probably consistent with relatively low content of As in hematite (≤2.9 wt.% As_2O_5; $n = 3$).

The Fe-As-Si-Al 'gels' (Raman spectra R3; Fig. S3) span all compositions from almost pure SiO_2-Al_2O_3 to compositions comparable to those of scorodite or bukovskýite (cf. Majzlan et al., 2012b). A characteristic feature of these gels is a diffuse variation in the content of the major elements (Fig. 4). The halloes of Si and Al around quartz and sheet silicate grains indicate the gradual dissolution of these minerals under acidic conditions. The gels recrystallize with time to porous aggregates of bukovskýite which contain no grains of silicates at all.

4.3. Sequential selective extractions

Results of SEP reveal similar patterns in the chemical fractionation of As between the samples of mining wastes (Fig. 5; full set of numerical result are given in Table S3, including data for As and Fe). For all samples, the majority of As was extracted by oxalate in the dark (F3: 46–80%, $\bar{x}$: 61%); slightly lower proportion of As was extracted by hot oxalate under light illumination (F4: 10–48%, $\bar{x}$: 24%). Maximum proportions of As in the (F1) water, (F2) phosphate, and (F5) $KClO_3$/HCl/HNO_3 extractions were significantly lower and corresponded only to 2.5% ($\bar{x}$: 0.6%), 13% ($\bar{x}$: 10%), and 11% ($\bar{x}$: 5%) of the total As.

4.4. Pore-water chemistry

Interaction of rain water with highly weathered and oxidized mining waste in the profile C resulted in very acidic (pH 2.24–3.52; $\bar{x}$: 2.84) and oxic (Eh ≥ 700 mV) pore water that contains high and variable concentration of Al (≤464 mg L^{-1}, $\bar{x}$: 113 mg L^{-1}), As (≤24.0 mg L^{-1}, $\bar{x}$: 2.53 mg L^{-1}), Ca (≤572 mg L^{-1}, $\bar{x}$: 500 mg L^{-1}), Cu (≤116 mg L^{-1}, $\bar{x}$: 23.6 mg L^{-1}), Fe (≤269 mg L^{-1}, $\bar{x}$: 57.5 mg L^{-1}), Si (≤82.0 mg L^{-1}, $\bar{x}$: 43.9 mg L^{-1}), SO_4^{2-} (≤4300 mg L^{-1}, $\bar{x}$: 2170 mg L^{-1}), and Zn (≤139 mg L^{-1}, $\bar{x}$: 16.2 mg L^{-1}) (Table S4). Aqueous concentrations of other elements were usually low (Cl ≤ 22.2 mg L^{-1}, K ≤ 1.13 mg L^{-1}, Na ≤ 15.5 mg L^{-1}, Pb ≤ 0.05 mg L^{-1}). Although the highest dissolved concentrations of the metal(loid)s were generally observed in the deeper parts of the waste profile (≥320 cm), their distribution significantly varied within the individual intervals previously used for collection of the solid samples (e.g. concentration of As between 0.50 and 24.0 mg L^{-1} or Fe (III) between 28 and 428 mg L^{-1} in the C350 sample; Table S4), implying a significant role of highly localized waste environments for the

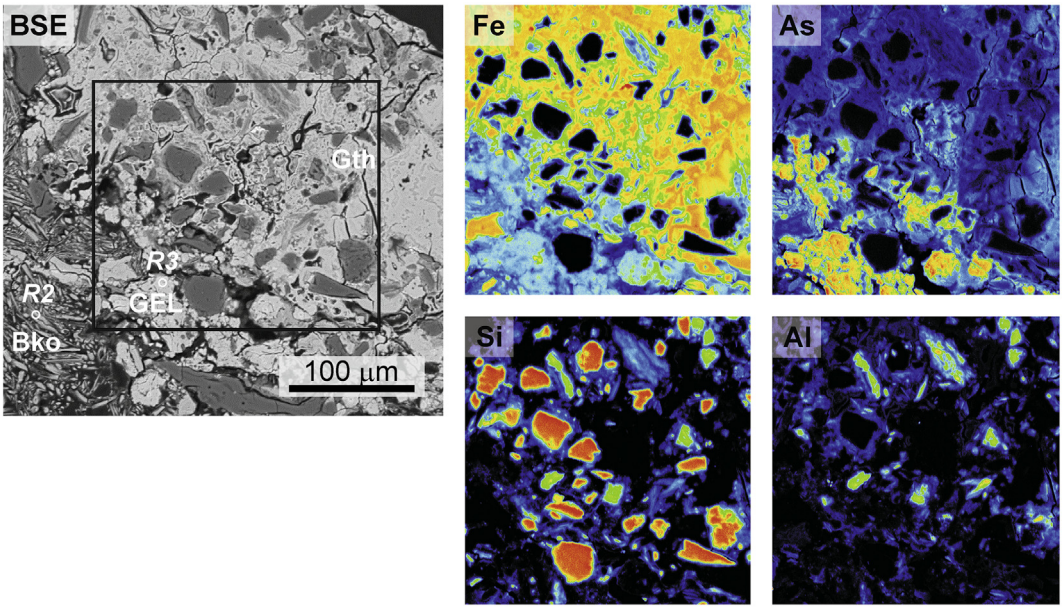

Fig. 4. Back-scattered electron (BSE) image of an assemblage of secondary minerals from Kaňk and element distribution maps for four selected elements. The area scanned for the elemental distribution is shown in the BSE image by a black rectangle. It consists of a mélange of the gel (GEL), goethite (Gth), quartz, and sheet silicates. The lower left corner of the BSE image shows an aggregate of acicular crystals of bukovskýite (Bko). Note the diffuse, patchy variations in the elemental concentrations of the major elements. Raman spectra obtained from locations *R2* and *R3* are given in (Fig. S3).

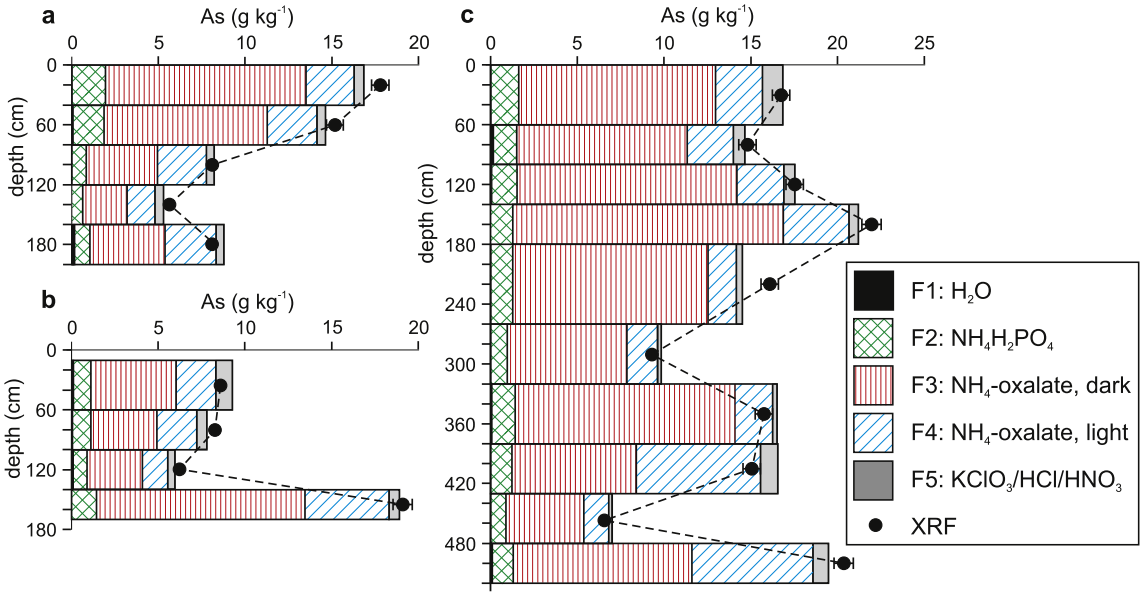

Fig. 5. Chemical fractionation of As in three mining wastes profiles (A, B, and C) from Kaňk obtained by sequential extraction analysis. Total As concentration was determined by energy dispersive X-ray fluorescence (XRF) spectrometry.

metal(loid)s mobility. Iron is mostly present as Fe(III) (> 80% of the total Fe) with the exception of seven samples with relatively low total dissolved Fe (Fe(II): 23–70% of the total Fe).

5. Discussion

Mineralogical composition of the mining waste, determined by powder X-ray diffraction, electron microprobe analyses and Raman spectroscopy, is relatively simple. The principal arsenic carriers are bukovskýite, scorodite, HFA, Fe (oxyhydr)oxides, and jarosite. There are subtle differences in the arsenic mineralogy between the samples from different profiles. The profiles A and C are similar but unlike the profile B. The profile B is dominated by Fe arsenates and lacks Fe sulfoarsenates (Fig. 4), likely because the waste materials in the B profile display higher pH and lower sulfate than other waste environments examined in this study (Table S2).

The relative proportions of principal arsenic minerals are very difficult to establish because of the heterogeneity of the mining waste. Bukovskýite, sometimes with minor amounts of scorodite, HFA, and jarosite, forms nodules and concretions of centimeter to decimeter size. Additional vertical and lateral variations essentially preclude collection of representative samples. A rough estimate of the proportions of the arsenic carriers can be derived from the results of the sequential extractions.

If the oxalate-promoted dissolution of the secondary arsenic minerals in complex mining waste samples congruently releases Fe and As, then their molar ratios may roughly estimate the relative proportion of As bound to Fe (sulfo)arsenates and Fe (oxyhydr)oxides or (hydroxy)

sulfates. Theoretical Fe/As molar ratios for the identified (sulfo)arsenate phases (bukovskýite, HFA, scorodite) are between 1.2 and 2.1 whereas these ratios for As-bearing Fe (oxyhydr)oxides and (hydroxy) sulfates were always higher (ferrihydrite, goethite, and schwertmannite ~13, jarosite ~54; calculated from EMP analyses). The Fe/As ratio in the liquid extracts varied from 2.3 to 6.1 ($\bar{x}$: 3.5) in F3 and from 4.3 to 40 ($\bar{x}$: 20) in F4. These values correspond to the dominant association of As with amorphous and poorly-crystalline (sulfo)arsenates such as HFA and bukovskýite (estimated at 80% of As in the oxalate in the dark), with a relatively low proportion of As associated with ferrihydrite and schwertmannite. Higher Fe/As molar ratios in F4 probably correspond to effect of jarosite dissolution.

These findings suggest that As in the mining waste samples is almost exclusively (≥85% of the total As; sum of the first 4 fractions in the SEP) associated with Fe(III) (oxyhydr)oxides, (hydroxy)sulfates, and (sulfo)arsenates, from which poorly-crystalline and oxalate-reactive forms (As-HFO, schwertmannite, bukovskýite, HFA, kaňkite, and zýkaite) dominate (Drahota et al., 2014). Well-crystalline and less-reactive forms (goethite, hematite, jarosite, and scorodite) are less common (Cornell and Schwertmann, 1996; Drahota et al., 2014). Proportion of As associated with sulfide and other oxalate-insoluble phases (F5) was always lower than 11% of the total As.

Reactivity of the mining waste with weakly concentrated aqueous solutions (e.g., rain water) is documented not only by the sequential extractions but also by the liquid samples collected in the field. Their low pH and high ionic strength are generated by episodic dissolution of the mining waste. Only two pore-water samples (depth of 320–380 cm) are saturated with respect to bukovskýite ($-5.2 \le SI \le 1.9$), but most of them are saturated with respect to scorodite ($-1.6 \le SI \le 2.2$) (undersaturation observed in depths < 100 cm). Less common Fe(III) (sulfo)arsenates kaňkite and zýkaite, also known from the site studied (Kocourková-Víšková et al., 2015) but not detected in our samples, display mild undersaturation ($-3.5 \le SI_{(kaňkite)} \le 0.3$; $-4.4 \le SI_{(zýkaite)} \le 0.1$). Two clusters of the measured variables, described below, conform well with the mineralogy of the waste.

The first cluster comprises As, Fe(III), and pH with a high mutual correlation ($R^2 \ge 0.65$, $p < 0.001$; Fig. S4) that is compatible with the strong association of Fe and As in the solid Fe(III) (oxyhydr)oxides, hydroxysulfates, and (sulfo)arsenates and their pH-dependent dissolution. The As(V) molalities, when plotted against pH, fall near the solubility curve for As-HFO (arsenical hydrous ferric oxide), not that of scorodite or bukovskýite (Fig. 6). The curves shown in Fig. 6 were calculated from thermodynamic data for the ferric arsenate phases, As-HFO (Majzlan, 2011), scorodite (Majzlan et al., 2012a), and bukovskýite (Majzlan et al., 2012b). They assume only dissolution of the given phase and do not consider the possibility of precipitation of other phases. Such processes were inspected by Majzlan et al. (2012a) and were shown to account for some observations regarding the solubility of arsenic at polluted sites. They operate, however, when phases formed under acidic solutions are exposed to mildly acidic or neutral solutions and this is not the case at the site studied here.

Hence, geochemical modeling shows that Fe and As in the aqueous solutions are most likely controlled by As-HFO (Fig. 6). The small but noticeable difference between the data (red diamonds in Fig. 6) and the calculated solubility curves for As-HFO can be explained by the fact that the composition, and hence also thermodynamic properties, of As-HFO are variable. Majzlan (2011) measured the thermodynamic properties of four different As-HFO compositions; all four corresponding curves are plotted. Additional variations in properties, including the thermodynamic ones, comes from incorporation of phosphate (quantified by Majzlan, 2011) but also ternary Fe-Ca-AsO_4 complexes (not quantified) and other chemical moieties. Moreover, in a collection of > 600 chemical analyses of mine drainage waters, all of them are slightly supersaturated with respect to As-HFO (see Fig. 3e in Majzlan et al., 2016). As-HFO, when forming, tends to be in equilibrium with the aqueous solution; the observed supersaturation can be probably

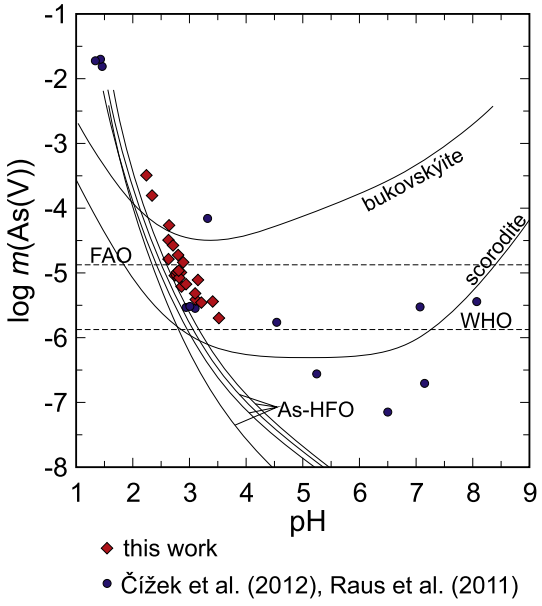

Fig. 6. pH and aqueous molality of As(V) in the samples from lysimeters (this work) and monitoring wells (Table S5; Čížek et al., 2012; Raus et al., 2011) at Kaňk. The dashed horizontal line marked "WHO" shows the drinking water limit (0.01 mg As/L) of the World Health Organization (WHO). The dashed horizontal line marked "FAO" shows the irrigation water limit (0.10 mg As/L) of the Food and Agriculture Organization.

assigned to the deficiencies in the sample preparation, namely the filtration of the aqueous samples. Using either 0.45 or 0.2 μm filters, some colloidal matter still passes into the analyzed samples and is responsible for the apparent supersaturation (cf. Nordstrom and Ball, 1989). This effect could be also the cause of the difference between the data points and curves in Fig. 6.

The second cluster of variables includes Al, Ca, Cd, Cu, Mg, Mn, Si, Zn, and SO_4 (Fig. S4). Gypsum is near saturation ($-0.1 \le SI \le 0.4$) in all samples from the lysimeters. Precipitation of this mineral seems to control the Ca concentration in water but the dissolved SO_4 is present in significant excess with respect to gypsum stoichiometry (aqueous Ca/SO_4 molar ratio is 0.62 ± 0.19, $\bar{x} \pm \sigma$). This excess is caused by the large amount of weathered sulfides that could not have been compensated by carbonates. A strong correlation between SO_4 and Al ($R^2 = 0.94$, $p < 0.001$) may suggest significant role of Al (hydroxy) sulfates such as alunogen ($Al_2(SO_4)_3{\cdot}17H_2O$) and aluminite ($Al_2SO_4(OH)_4{\cdot}7H_2O$) (soluble (hydroxy)sulfates that were identified in the mining waste (Pauliš, 1993). Contribution of Cu, Zn, and Mg may be related to highly-soluble chalcantite (Pauliš, 1993) and boyleite ($(Zn,Mg)SO_4{\cdot}4H_2O$) (Pauliš et al., 2015) that are rarely present in the mining waste. The strong correlation between Al and Cu ($R^2 = 0.99$), Zn ($R^2 = 0.89$), and other metals (Fig. S4) may also reflect their high affinity to Al (hydroxy)sulfate (Carrero et al., 2015).

Hence, Fe and As in the mining waste at Kaňk is stored in reactive but not highly soluble minerals such as As-HFO, bukovskýite, HFA, and iron oxides. The solubility of these two elements is controlled by As-HFO. A smaller fraction of Fe and As is contained in less reactive scorodite or jarosite. Jarosite also appears to be the main reservoir of Pb. The elements Ca, Al, Zn, and Cu are transported through wetting-drying cycles as ephemeral sulfates, found at the studied site (Pauliš, 1993; Pauliš et al., 2015). These findings agree well with the visual observation that the old dumps turn white after each precipitation event, probably owing to crystallization of gypsum. After a few days, the color changes to the usual yellowish-beige. Some of the Cu and Zn is also stored in iron oxides.

6. Conclusion

The historical dumps at Kaňk are deeply weathered and supplied regularly by uncontaminated rain water. Many of these dumps, located in a flat, soft relief around the municipality of Kutná Hora, are clay-rich and retain the rain water for a prolonged period of time. This retention capacity is much different from many other historical dumps which are rocky and water flushes quickly through them. The eye-catching minerals bukovskýite, kaňkite, and zýkaite store and release As and Fe at Kaňk but the mobility of these elements is controlled, as just at many sites around the world, by the unspectacular arsenic-loaded hydrous ferric oxides. High amount of sulfate in the percolating fluids is partially contained by gypsum and Al-Cu-Zn sulfates of transient nature. By the capillary action, these sulfates form ephemeral efflorescence on the dump, only to be washed away by the next rain. Some of the water, however, reaches the shallow, laterally restricted aquifers and contaminates them with arsenic (Čížek et al., 2012; Raus et al., 2011). Concentrations of up to 1440 mg L^{-1} As, measured in one of the monitoring wells installed directly in the mining waste material, are alarming, but the migration of the contaminants from this isolated aquifer seems to be limited due to impermeable bedrock (Čížek et al., 2012).

Taking the area of the dumps of 3000 m^2 with the average annual precipitation of 580 mm and the median arsenic concentration in the dump water (0.765 mg/L, this work), the total arsenic budget transported annually is 1330 kg. This value needs to be seen as the upper limit because some of the rain water evaporates or could be uptaken by the plants. Yet, this value, when compared to the few hundred thousands tones of the mining waste in the dumps with an average of 1% As in dry weight (Table S2) shows that the dumps have the potential of releasing similar amounts of arsenic as today for thousands of years.

At pH above ~2.8, the hydrous ferric oxide maintain the aqueous arsenic concentration below 0.10 mg/L, the limit set by the Food and Agriculture Organization for irrigation water. Below this pH, the percolation water contains high concentrations of arsenic, comparable to the highest concentrations detected in the heavily polluted shallow wells in West Bengal and Bangladesh (see Fig. 2 in Chowdhury et al., 2000). The groundwater in the dumps at Kaňk is, however, never used for drinking; it may be occasionally used for irrigation of private gardens and crops, though. Therefore, an immediate remediation solution could be a slight increase of pH, at least above 3. It is not clear if this measure would also suppress the formation of the extremely arsenic-rich underground water (up to 1440 mg L^{-1} As, see above).

Acknowledgments

We appreciate the constructive review of Dave Craw that helped to improve this manuscript. This work was funded by the Czech Science Foundation (GAČR) Grant 16-09352S and the DFG Graduate College GRK 1257/1. The corresponding author's team was also supported by the Operational Program Prague - Competitiveness (Project No. CZ.2.16/3.1.00/21516). Laboratory assistance was provided by Adam Culka, Lenka Jílková, Martin Mihaljevič, František Veselovský, Michaela Fridrichová, Stefan Kiefer, and Zuzana Korbelová.

Appendix A. Supplementary data

Supplementary data related to this article can be found at https://doi.org/10.1016/j.apgeochem.2018.08.029.

References

Blowes, D.W., Ptacek, C.J., Jambor, J.L., Weissner, C.J., Paktunc, D., Gould, W.D., Johnson, D.W., 2013. The geochemistry of acid mine drainage. In: second ed. In: Holland, H.D., Turekian, K.K. (Eds.), Treatise on Geochemistry, vol 11. pp. 131–190.

Burton, E.D., Bush, R.T., Johnston, S.G., Watling, K.M., Hocking, R.K., Sullivan, L.A., Parker, G.K., 2009. Sorption of arsenic(V) and arsenic(III) to schwertmannite. Environ. Sci. Technol. 43, 9202–9207.

Carrero, S., Pérez-López, R., Fernandez-Martinez, A., Cruz-Hernández, P., Ayora, C., Poulain, A., 2015. The potential role of aluminium hydroxysulphates in the removal of contaminants in acid mine drainage. Chem. Geol. 417, 414–423.

Casiot, C., Leblanc, M., Bruneel, O., Personné, J.-C., Koffi, K., Elbaz-Poulichet, F., 2003. Geochemical processes controlling the formation of As-rich waters within a tailings impoundments (Carnoulès, France). Aquat. Geochem. 9, 273–290.

Čech, F., Jansa, J., Novák, F., 1976. Kaňkite, $FeAsO_4{\cdot}3.5H_2O$, a new mineral. Neues Jahrbuch Mineral. Monatsh. 9, 426–436.

Čech, F., Jansa, J., Novák, F., 1978. Zýkaite, $Fe_4^{3+}(AsO_4)(SO_4)(OH){\cdot}15H_2O$, a new mineral. Neues Jahrbuch Mineral. Monatsh. 3, 134–144.

Chowdhury, U.K., Biswas, B.K., Chowdhury, T.R., Samanta, G., Mandal, B.K., Basu, G.C., Chanda, C.R., Lodh, D., Saha, K.C., Mukherjee, S.K., Roy, S., Kabir, S., Quamruzzaman, Q., Chakraborti, D., 2000. Groundwater arsenic contamination in Bangladesh and West Bengal, India. Environ. Health Perspect. 108, 393–397.

Čížek, J., Fojtík, S., Zuska, R., Vít, V., Vávra, J., 2012. Final Report of Exploration and Risk Assessment at OÚM ID0014 Šafary, Kutná Hora-kaňk. Technical Report, Geofond 1236/2011. (in Czech).

Cornell, R.M., Schwertmann, U., 1996. The Iron Oxides. VXH Verlagsgesellschaft mbH, Weinheim.

Culka, A., Kindlová, H., Drahota, P., Jehlička, J., 2016. Raman spectroscopic identification of arsenate minerals *in situ* at outcrops with handheld (532 nm, 785 nm) instruments. Spectrochim. Acta 154, 193–199.

Das, S., Essilfie-Dughan, J., Hendry, M.J., 2014. Arsenate adsorption onto hematite nanoparticles under alkaline conditions: effect of aging. J. Nanoparticle Res. 16. https://doi.org/10.1007/s11051–014-2490-3.

Drahota, P., Filippi, M., 2009. Secondary arsenic mineral in the environment: a review. Environ. Int. 35, 1243–1255.

Drahota, P., Grösslová, Z., Kindlová, H., 2014. Selectivity assessment of an arsenic sequential extraction procedure for evaluating mobility in mine wastes. Anal. Chim. Acta 839, 34–43.

Drahota, P., Knappová, M., Kindlová, H., Culka, A., Majzlan, J., Mihaljevič, M., Rohovec, J., Veselovský, F., Fridrichová, M., Jehlička, J., 2016. Mobility and attenuation of arsenic in sulfide-rich mining wastes from the Czech Republic. Sci. Total Environ. 557–558, 192–203.

Drahota, P., Raus, K., Rychlíková, E., Rohovec, J., 2018. Bioaccessibility of As, Cu, Pb, and Zn in mine waste, urban soil, and road dust in the historical mining village of Kaňk, Czech Republic. Environ. Geochem. Health 40, 1495–1512.

Dunn, P.J., 1982. New data for pitticite and a second occurrence of yukonite at Sterling Hill, New Jersey. Mineral. Mag. 46, 261–264.

Duquesne, K., Lebrun, S., Casiot, C., Bruneel, O., Personné, J.-C., Leblanc, M., Elbaz-Poulichet, F., Morin, G., Bonnefoy, V., 2003. Immobilization of arsenite and ferric iron by *Acidithiobacillus ferrooxidans* and its relevance to acid mine drainage. Appl. Environ. Microbiol. 69, 6165–6173.

Egal, M., Casiot, C., Morin, G., Parmentier, M., Bruneel, O., Lebrun, S., Elbaz-Poulichet, F., 2006. Kinetic control on the formation of tooleite, schwertmannite and jarosite by *Acidithiobacillus ferrooxidans* strains in an As(III)-rich acid mine water. Chem. Geol. 265, 432–441.

Filippi, M., Machovič, V., Drahota, P., Böhmová, V., 2009. Raman microspectrometry as a valuable additional method to X-ray diffraction and electron microscope/microprobe analysis in the study of iron arsenates in environmental samples. Appl. Spectrosc. 63, 621–626.

Filippi, M., Drahota, P., Machovič, V., Böhmová, V., Mihaljevič, M., 2015. Arsenic mineralogy and mobility in the arsenic-rich historical mine waste dump. Sci. Total Environ. 536, 713–728.

Gieré, R., Sidenko, N.V., Lazareva, E.V., 2003. The role of secondary minerals in controlling the migration of arsenic and metals from high-sulfide wastes (Berikul gold mine, Siberia). Appl. Geochem. 18, 1347–1359.

Havlíček, J., Pácal, Z., 1962. Arsenic in mine water from the Staročeské zone (Kaňk near Kutná Hora). Čas. mineral. geol. VII, 260–268 (in Czech).

Holub, M., Hoffman, V., Mikuš, M., Trdlička, Z., 1982. Polymetallic mineralization of the Kutná Hora ore district. Sbor. geol. Věd - Lož. geol. mineral. 23, 60–123 (in Czech).

Jambor, J.L., 2003. Mine-waste mineralogy and mineralogical perspectives of acid-base accounting. In: Jambor, J.L., Blowes, D.W., Ritchie, A.I.M. (Eds.), Environmental Aspects of Mine Wastes. Mineral. Assoc. Can., Short Course Handbook 31, pp. 117–145.

Jia, Y., Xu, L., Fang, Z., Demopoulos, G.P., 2006. Observation of surface precipitation of arsenate on ferrihydrite. Environ. Sci. Technol. 40, 3248–3253.

Kocourková-Víšková, E., Loun, J., Sracek, O., Houzar, S., Filip, J., 2015. Secondary arsenic minerals and arsenic mobility in a historical waste rock piles at Kaňk near Kutná Hora, Czech Republic. Mineral. Petrol. 109, 17–33.

Kořan, J., 1950. History of mining in the Kutná Hora ore district, Vědecko-technické nakladatelství. Geotechnica 11 (in Czech).

Langmuir, D., Mahoney, J., Rowson, J., 2006. Solubility products of amorphous ferric arsenate and crystalline scorodite ($FeAsO_4{\cdot}2H_2O$) and their application to arsenic behavior in buried mine tailings. Geochem. Cosmochim. Acta 70, 2942–2956.

Loun, J., Čejka, J., Sejkora, J., Plášil, J., Novák, M., Frost, R.L., Palmer, S.J., Keeffe, E.C., 2011. A Raman spectroscopic study of bukovskýite $Fe_2(AsO_4)(SO_4)(OH){\cdot}7H_2O$, a mineral phase with a significant role in arsenic migration. J. Raman Spectrosc. 42, 1596–1600.

Majzlan, J., 2011. Thermodynamic stabilization of hydrous ferric oxide by adsorption of phosphate and arsenate. Environ. Sci. Technol. 45, 4726–4732.

Majzlan, J., Drahota, P., Filippi, M., Grevel, K.-D., Kahl, W.-A., Plášil, J., Boerio-Goates, J., Woodfield, B.F., 2012a. Thermodynamic properties of scorodite and parascorodite ($FeAsO_4{\cdot}2H_2O$), kaňkite ($FeAsO_4{\cdot}3.5H_2O$), and $FeAsO_4$. Hydrometallurgy 117–118,

47–56.
Majzlan, J., Lazic, B., Armbruster, T., Johnson, M.B., White, M.A., Fisher, R.A., Plášil, J., Loun, J., Škoda, R., Novák, M., 2012b. Crystal structure, thermodynamic properties, and paragenesis of bukovskýite, $Fe_2(AsO_4)(SO_4)(OH)\cdot 9H_2O$. J. Mineral. Petrol. Sci. 107, 133–148.
Majzlan, J., Drahota, P., Filippi, M., 2014. Parageneses and crystal chemistry of arsenic minerals. Rev. Mineral. Geochem. 79, 254–258.
Majzlan, J., Amoako, F.Y., Kindlová, H., Drahota, P., 2015. Thermodynamic properties of zýkaite, a ferric sulfoarsenate. Appl. Geochem. 61, 294–301.
Majzlan, J., Števko, M., Lánczos, T., 2016. Soluble secondary minerals of antimony in Pezinok and Kremnica (Slovakia) and the question of mobility or immobility of antimony in mine waters. Environ. Chem. 13, 927–935.
Malec, J., Pauliš, P., 1997. Environmental impact of historical mining and smelting at the Kutná Hora ore district. Bull. Mineral.-Petrol. Odd. NM v Praze 4–5, 84–105 (in Czech).
Morin, G., Juillot, F., Casiot, C., Bruneel, O., Personné, J.-C., Elbaz-Poulichet, F., Leblanc, M., Ildefonse, P., Calas, G., 2003. Bacterial formation of tooeleite and mixed arsenic (III) or arsenic(V)-iron(III) gels in the Carnoulès acid mine drainage. A XANES, XRD, and SEM study. Environ. Sci. Technol. 37, 1705–1712.
Müller, K., Ciminelli, V.S.T., Dantas, M.S.S., Willscher, D., 2010. A comparative study of As(III) and As(V) in aqueous solutions and adsorbed on iron oxy-hydroxides by Raman spectroscopy. Water Res. 44, 5660–5672.
Nordstrom, D.K., Ball, J.W., 1989. Mineral saturation states in natural waters and their sensitivity to thermodynamic and analytical errors. Sci. Geol. Bull. 42, 269–280.
Nordstrom, D.K., Wilde, F.D., 2005. Reduction-oxidation potential (electrode method). U.S. Geological survey techniques of water-resources investigations, Book 9, chap. A6, section 6.5. Available from: https://water.usgs.gov/owq/FieldManual/Chapter6/6.5_v_1.2./.
Nordstrom, D.K., Alpers, C.N., Ptacek, C.J., Blowes, D.W., 2000. Negative pH and extremely acidic mine waters from Iron Mountain, California. Environ. Sci. Technol. 34, 254–258.
Novák, F., Povondra, P., Vtělenský, J., 1967. Bukovskýite, $Fe_2^{3+}(AsO_4)(SO_4)(OH).7H_2O$, from Kaňk, near Kutná Hota – a new mineral. Acta Univ. Carol. Geol. 4, 297–325 (in Czech).
Ondruš, P., Skála, R., Viti, C., Veselovský, F., Novák, F., Jansa, J., 1999. Parascorodite, $FeAsO_4{\cdot}2H_2O$ – a new mineral from Kaňk near Kutná Hora, Czech Republic. Am. Mineral. 84, 1439–1444.
Parkhurst, D.L., Appelo, C.A.J., 1999. User's Guide to PHREEQC (Version 2) – a Computer Program for Speciation Batch-reaction, One-dimensional Transport, and Inverse Geochemical Calculations. U.S. Geological Survey Water-Resource Investigations Report, 99–4259.
Pauliš, P., 1993. Secondary sulfates at Kaňk near Kutná Hora. Věst. Čes. Geol. Úst. 68, 47–48 (in Czech).
Pauliš, P., Malíková, R., Pour, O., 2015. Boyleite from medieval dumps of the Staročeské lode at Kaňk near Kutná Hora (Czech Republic). Bull. mineral-petrolog. Odd. Nár. Muz. 23, 43–45 (in Czech).
Raus, M., Bílek, O., Fulková, J., Hájek, M., Holub, M., Křenová, Z., Nekl, M., Zuska, R., Zýval, V., 2011. Final Report of Exploration and Risk Assessment at OÚM ID0017 Kuntery, Kutná Hora-kaňk. Technical Report, Geofond 1236/2011. (in Czech).
Williams, M., 2001. Arsenic in mine waters: an international study. Environ. Geol. 40, 267–278.
Yu, J.Y., Heo, B., Choi, I.K., Cho, J.P., Chang, H.W., 1999. Apparent solubilities of schwertmannite and ferrihydrite in natural stream waters polluted by mine drainage. Geochem. Cosmochim. Acta 63, 3407–3416.